



## **TENSION AND COMPRESSION MICROPILE LOAD TESTS IN GRAVELLY SAND**

**Armin W. Stuedlein**  
Hart Crowser, Inc.  
Seattle, Washington (USA) 98109

**Matt D. Gibson**  
Hart Crowser, Inc.  
Seattle, Washington (USA) 98109

**Garry E. Horvitz**  
Hart Crowser, Inc.  
Seattle, Washington (USA) 98109

### **ABSTRACT**

Micropiles were selected for several upgrades to a paper machine at the Nippon Paper Industries USA Company in Port Angeles, Washington. This paper presents several aspects of the micropile design and subsequent load test performance for two separate upgrades at the paper mill. The micropile load tests, performed in tension and compression, provide a reference for micropile performance in medium dense to dense, gravelly sand. Comparison of the load test performance suggests that the common assumption of disregarding the contribution of end-bearing resistance may be overly conservative. The load test performance is interpreted in the framework of a simple, global stiffness degradation technique, which provides an estimate of load transfer without the use of strain gages. The analyses suggest that the mode of loading (e.g., tension or compression) influences the average load transfer properties for the small diameter micropiles.

### **INTRODUCTION**

Nippon Paper Industries USA Company, located on the Olympic Peninsula along the Strait of Juan de Fuca, in Port Angeles, Washington, owns and operates a large paper mill. The plant was originally constructed and put into service in the early 1920's, with numerous modernizations and upgrades throughout the eighty plus years of operation. Due to production requirements, the paper mill operates two paper machines 362 to 363 days a year, 24 hours a day, and produces high quality recycled paper product for global use and distribution. Since maintaining the rate of paper production is of paramount importance, periods of maintenance and upgrading must be kept to extremely short durations. The necessity of quick installation of foundation members coupled with very low headroom for equipment led to the selection of micropiles for the support of new structural loads. This paper presents the design and load test performance of the micropile foundation systems employed for two separate upgrades of the paper mill.

### **PROJECT DESCRIPTION**

Two periods of maintenance and upgrades for Paper Machine Number Two (PM2) occurred in Autumn 1991 (Upgrade 1) and Spring of 2007 (Upgrade 2). In 1991, PM2 required the placement of a saveall filtration unit, which increases the rate of pulp fiber recovery for reuse, an important part of efficient paper production. Upgrades for PM2 that occurred in 2007 included the replacement of the paper press and dryer systems, which are required for product finishing.

New equipment commissioned for the upgrades required structural support and foundation load capacity above that available from the existing structural and foundation members. In addition, the existing structural and foundation components were required to stay in service during the upgrades to support the portions of the paper machine not being serviced. The existing foundation system consisted of the original timber piles driven in the 1920's, tied to mass concrete pile caps.

### **GEOLOGY & SUBSURFACE CONDITIONS**

The project site is set just north of the Olympic Mountains directly on the Strait of Juan de Fuca. The current regional topography and geology is the result of the last advance and retreat of the Cordilleran Ice Sheet, known as the Vashon Stade of the Frasier Glaciation (Armstrong, et al, 1965). The maximum height of ice during the Vashon Stade at Port Angeles was approximately 1000 m (3280 feet) and occurred between 18,000 to 15,000 years before present (Booth, 1987; Porter and Swanson 1998) in the Pleistocene. The Nippon Paper plant is located on the western edge of a natural spit, called Ediz Hook, which provides a barrier to form Port Angeles Harbor. Ediz Hook is approximately 5 km (3 mi) long and 40 m (130 feet) wide at its narrowest point. Ediz Hook has been dated to approximately 5,000 years before present and likely developed as a result of wave action and high energy deltaic discharge from the nearby Elwha River delta (Downing, 1983; Galster, 1989).

Ediz Hook spit is largely comprised of medium dense to very dense, Quaternary and Holocene sand and gravel beach deposits (Qb and Hb, respectively), grading to dense to very dense, glacially overridden gravelly, silty sand advance

Upgrade 1

Upgrade 1, occurring in 1991, was performed to install the saveall filtration unit. The structural loads to be supported by the new foundations included 356 kN (80 kips) column loads and a 5 kPa (100 psf) floor load. The original foundation alternative recommended for the support of the new structural loading was the use of 406 mm (16 inch) diameter augercast piling. The proposed length of augercast piling was 6.4 m (21 feet), extending to elevation -1.8 m (-6 feet). A contractor, citing the improved ability of equipment maneuverability, reduced headspace requirement, and quicker installation, bid on the work plan with a micropile alternative. The alternative work plan was reviewed and approved for construction.

Although a variety of pile cap geometries exist throughout the paper mill complex, the typical pile cap was square in shape and 1.68 m (5.5 feet) wide, consisting of five timber piles. Columns were generally centered on the cap and central timber pile, spaced at 6.1 m (20 feet) on center. Upgrade 1 required the installation of nine micropiles to increase the structural capacity of three existing pile caps/groups. Two plumb and three battered micropiles were installed between two separate, adjacent pile caps for the support of two new columns. The piles were tied to the two adjacent pile caps to form a monolithic pile cap with dimensions 4.1 m (13.5 feet) wide by 6.1 m (20 feet) long. Four plumb micropiles were installed adjacent to an existing pile group to form an approximately square, 3.35 m (11 feet) wide pile cap. New micropiles were centered to provide a minimum spacing of 1.2 m (4 feet), and offset a minimum of 0.9 m (3 feet) from existing timber piles.

Upgrade 2

Upgrade 2, occurring in 2007, was performed to replace the paper press and dryer systems. The maximum structural loads to be supported by the new deep foundation elements included 356 kN (80 kips) column loads. Based on the performance of the micropiles during Upgrade 1, micropiles of similar cased and bond zone length were proposed for Upgrade 2.

Columns in the location of Upgrade 2 were approximately 6.1 m (20 feet) by 4.8 m (15.7 feet). Ten plumb micropiles were installed between four existing pile caps for the support of six new columns and structural supports. New micropiles were centered to provide a minimum spacing of 1.1 m (3.5 feet) from both new and existing piling.

Micropile Design and Installation

For both upgrades, the micropiles were contracted as design-build, with review of contractor design submittal by the clients' structural and geotechnical engineers. The first task of construction consisted of coring a 0.61 m (2 foot) diameter hole through the existing 1 m (3.3 feet) thick floor slab and

outwash (Qva). The subsurface corresponding to the micropile load tests is comprised of about 1.52 m (5 feet) of silty, gravelly sand fill, over 10.67 m (35 feet) of medium dense to dense, gravelly sand grading to sandy gravel including occasional cobbles (beach deposits), over very dense, slightly gravelly sand (advance outwash). Representative grain size distributions for soil units are shown in Fig 1, whereas the SPT blow counts for the boring nearest the load tests are shown in Fig 2.

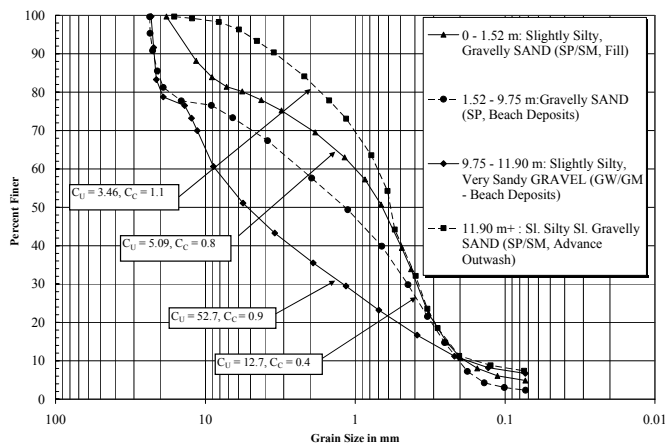


Fig. 1. Grain size distribution for site subsurface.

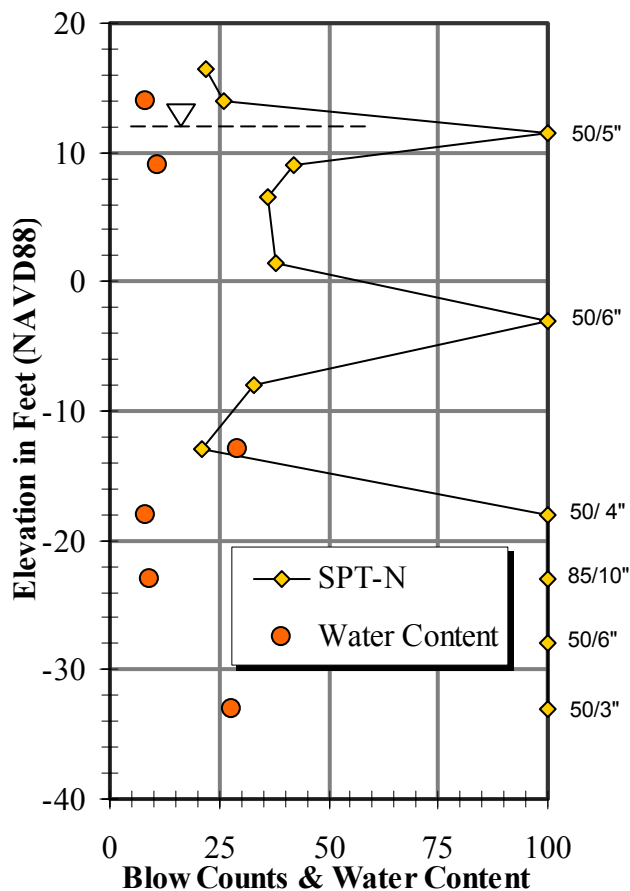


Fig. 2. Results of SPT boring closest to tested micropiles.

pile cap. Holes were advanced with a limited access drill rig with remote power source and water supply. Production micropiles included 9.1 m (30 foot) long, #11 Grade 75 thread bar, with extra length providing tie-in with existing floor slab and pile cap. Micropiles tested used Grade 150 steel to safely handle the test loads. The casing was 140 mm (5.5 inch) diameter, with 13 mm (0.5 inch) thick wall, N80 steel pipe. The cased zone was 3.05 m (10 feet) length, with a 5.2 m (17 feet) long bond zone for all production micropiles for both upgrades. Double corrosion protection was specified and installed for the full length of the micropile excluding the slab and cap embedment. A minimum of two centralizers were required for the steel reinforcement.

In general, very rough drilling was encountered. Typical drilling durations spanned 1.5 to 4 hours, with exceptionally tight drilling conditions at depth within the coarser, gravelly sand and sandy gravel. The hole was advanced in 0.9 m (3 foot) pipe sections, with pressurized water jetting to assist in advancement of the casing and cuttings removal. Grout, specified with a water-cement ratio no more than 0.45, was pumped at pressures ranging from 0.5 to 0.8 MPa (65 to 120 psi) during casing withdrawal. The grout level of the completed Type B (FHWA, 2005) micropiles were observed for the purpose of topping off grout level as required. Grout volumes typically ranged between 2 and 5x the theoretical volume, indicative of the very porous nature of the beach deposits. No micropile was allowed to be installed within 2 meters (6.5 feet) or 14 diameters of a micropile installed up to 24 hours prior. This requirement limited the occurrence of suspected grout communication to just one micropile installation of the approximately 20 installed at the project site. No records of grout breaks were available for Upgrade 1. For Upgrade 2, a three day grout break performed 12 hours prior to load testing yielded a compressive strength of 14.3 MPa (2080 psi). The Young's modulus, used in subsequently presented analyses, is estimated from the compressive strength data as approximately 17.9 MPa (2600 ksi).

## LOAD TEST SETUP, PROCEDURE, & DISCUSSION

A load test was specified for each upgrade. A compression load test was performed on a production micropile for Upgrade 1. Scheduling and geometrical considerations dictated the selection of a tension test on a production pile for Upgrade 2. The following discussion highlights the load test setup for each of the load tests.

### Compression Test

The compression test was performed on a production pile with a cased zone of 3 m (10 foot) length and a 5.2 m (17 foot) long bond zone. The reaction piles included one sacrificial micropile and one adjacent production pile. To ensure that adequate reaction force would be available, both reaction piles had a bond zone lengthened to 7.6 m (25 feet). The reaction piles were spaced 1.2 m (4 feet) on-center from the test micropile. Although greater spacing would have been

preferable, the cost associated with drilling two sacrificial piles for a job requiring no more than nine micropiles was deemed unjustified. Therefore, the consideration of interaction between the test and reaction piles may be warranted. Two dial gauges, with 0.001-inch resolution, were placed, diametrically opposed, on the rigid loading plate resting on the micropile and used to support the hydraulic jack.

### Tension Test

The tension test was performed on the first production pile installed during Upgrade 2. This micropile was placed as one of two single piles supplementing the exterior of one of the four pile caps being upgraded. Therefore, no other production piles could be employed to provide reaction during a compression load test. A compression test would have required two sacrificial micropiles in addition to the ten production piles, and therefore, a tension test was approved for performance verification.

One lift of cribbing, consisting of four, 150 mm (6-inch) square, pre-treated lumber pieces 1.5 m (5 feet) long was placed on either side of the micropile. Shims were then used to level the reaction frame and center it over the micropile. Following placement of the hydraulic jack around the steel reinforcement, two dial gauges were positioned over the bearing plate used to transmit the jack displacement to the steel reinforcement. Additionally, two dial gauges were positioned over the beam on either side of the jack, in order to observe and remove the effects of beam deflection. The free length of steel reinforcement used to span the length from the production pile head to the reaction frame was observed, with subsequent displacements during loading removed from the load-displacement curve presented herein.

### Load Test Procedures

For the compression load test, a seating load of 53 kN (12 kips) was applied prior to zeroing the dial gauges. Compressive load was applied in 5 cycles according to the schedule shown in Table 1. A seating load of 22 kN (5 kips) was applied to the micropile for the tension load test prior to zeroing the gauges. Load was applied in eight, 89 kN (20 kip) increments, to a maximum of 717 kN (160 kips), followed by unloading in four, 178 kN (40 kip) increments.

## MICROPILE PERFORMANCE

The results of the two micropile load tests are shown in Fig 3 side-by-side for comparison. It should be noted that the cased zone, the bond zone, and the elevation of the top of micropile are identical for both tests. A break in the compression load test curve is noted at a load of 310 kN (70 kips). This contrasts noticeably to the tension load test, where a strong change in behavior is noted a load of 179 kN (40 kips). The displacement of the micropiles at the design working load in compression and tension is approximately 1 and 5 mm (0.04

and 0.2 inch), respectively, indicating an extremely stiff response.

The results of the load tests in Fig 3 suggest fairly different behavior between elements loaded in tension and elements loaded in compression. End-bearing resistance of instrumented micropiles has been recently reported by Holman and Barkauskas (2007) and Han and Ye (2006). Based on Fig 3, the assumption of no contribution of end bearing resistance for micropiles loaded in compression appears to be conservative for micropiles founded within sand and gravel. Further investigation into the general behavior of these micropile test results is warranted.

Table 1. Compressive Test Load Schedule, in kN.

Load Number	Cycle 1	Cycle 2	Cycle 3	Cycle 4	Cycle 5
0	0	0	0	0	0
1	33	33	33	33	33
2	106	106	106	106	106
3		178	178	178	178
4		244	244	244	244
5			310	310	310
6			383	383	383
7				449	449
8				515	515
9					587
10					660

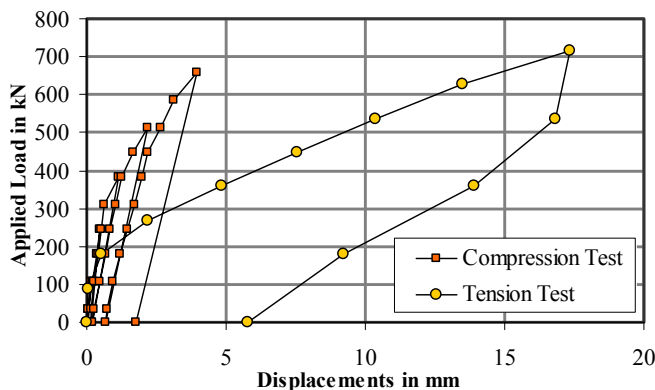


Fig. 3. Results of Compression and Tension Load Tests.

## ANALYSIS OF THE COMPRESSION LOAD TEST

### Compressive Micropile Behavior

For the purposes of assessing the performance of the compression load test, it is convenient to plot the results without showing the tension test. The base load-displacement data is shown with a load displacement curve corrected for the net or residual micropile head displacement at the end of each

load cycle in Fig 4. The compressive load displacement curves of micropiles have been successfully modeled with a hyperbolic curve by others (e.g., Jeon and Kulhawy, 2001). For the purposes of estimating the ultimate load, a modified hyperbolic curve was found to best fit the corrected compression load test data; the modified curve is given by

$$P = \frac{\Delta}{a^n + \left(\frac{b}{\Delta}\right)^n} \quad (1)$$

where  $P$  = applied load,  $\Delta$  = observed pile head displacement,  $a$  and  $b$  = curve fitting coefficients, and  $n$  = curve fitting exponent. The ultimate load for the compression test was found, by extrapolation, to be approximately 1440 kN (320 kips).

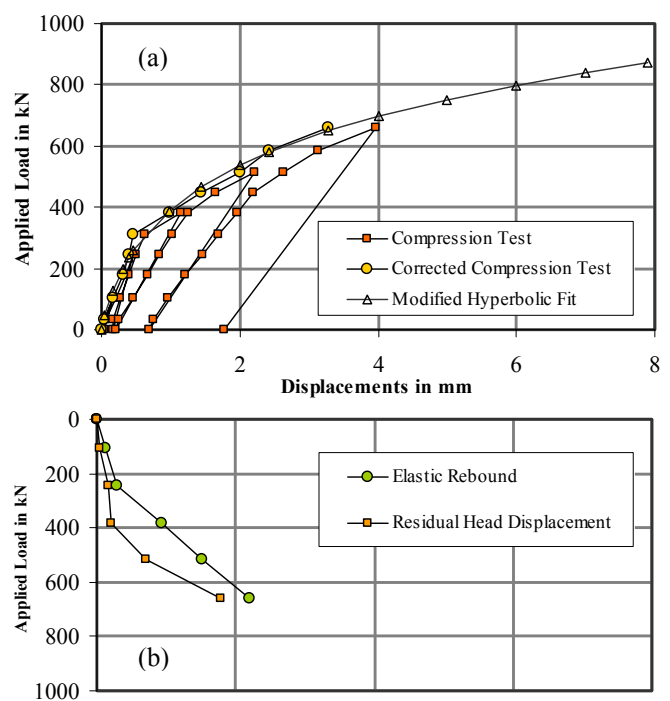


Fig. 4. Compression Load Test Data: (a) base load-displacement curve, corrected load-displacement curve, and fitted hyperbolic curve; (b) elastic and residual displacements.

Figure 4 presents the corrected load displacement curve, which represents the estimated virgin load displacement curve. The load-displacement data presented in this manner may provide a better estimate of the geotechnical performance of a monotonically loaded production micropile. The virgin load displacement curve is used for analyses presented below. Also shown in Fig 4 are the elastic rebound curve and residual micropile head displacement. The elastic rebound curve presents the noted recovered displacements upon the removal of load at the end of each load cycle. By inspection, the rate of residual micropile head displacement appears to increase nonlinearly with increasing load. The elastic recovery,

however, is best described by a bilinear relationship. This behavior is expected, given the difference in structural properties between the cased length and the bond zone. In fact, the slope of the elastic recovery curve prior to the break is greater than the stiffness of the cased length; subsequent to the break in the curve the axial stiffness approaches that of the weighted mean axial stiffness of the whole micropile. This behavior also implies that load transfer occurs within the cased zone; indeed, a possible implication provided by this data is that 70 percent of the design service load is transferred along the cased length. Some simple assumptions will allow a basic, yet instructive, estimation of load transfer along the length of the micropile.

### Load Transfer Models

The load transfer through micropiles is best studied with the use of instrumentation, including strain gages for the determination of incremental load transfer and toe load and movement, and tell-tales for verifying micropile toe movement. However, an estimation of load transfer is possible based upon simplifying assumptions regarding the development of loaded micropile length, rate of load transfer, and interface behavior. Several methods have been recently proposed, ranging from the fairly complicated (e.g., Misra, et al, 2004; and Zhu and Chang, 2002) to the simple (e.g., Jeon and Kulhawy, 2001; Cadden, et al, 2004). Although complicated models provide a realistic framework for understanding detailed load-transfer behavior, the practitioner often requires adjusting design bond lengths based on limited geotechnical information and in a time sensitive setting. Therefore, simple models, readily understood and employed, can provide use in a consulting environment.

A simple load transfer estimation technique is presented in Jeon and Kulhawy (2001), where a database of 21 micropile load tests were assembled and analyzed assuming load transfer along the bond length, only.

Table 2. Computed bond zone stresses and  $\beta$  values.

Test Data		Cased Beta = 0		Cased Beta = 1		Cased Beta = 2	
Displacement (mm)	Applied Load (kN)	Bond Zone Bond Stress (kPa)	Bond Zone Beta	Bond Zone Bond Stress (kPa)	Bond Zone Beta	Average Bond Stress (kPa)	Average Beta
0.00	0	0	0	0	0	0	0
0.05	33	13	0.17	0	0	0	0
0.17	106	43	0.53	30	0.37	13	0.16
0.30	178	72	0.90	62	0.77	45	0.56
0.41	244	99	1.23	91	1.13	74	0.92
0.47	310	125	1.56	120	1.49	103	1.28
0.98	383	155	1.92	152	1.89	135	1.68
1.45	449	181	2.25	181	2.25	164	2.04
2.01	515	208	2.59	210	2.61	193	2.40
2.43	587	237	2.95	242	3.00	225	2.80
3.28	660	267	3.32	273	3.40	257	3.19

Following the procedure outlined in Jeon and Kulhawy (2001), the bond stress within the bond zone was estimated and resulting value of Beta computed, where Beta equals the ratio of bond stress to mean vertical effective stress. The average bond stress was computed for three cases of casing interface load-transfer:

- Case 1: No load transfer through cased zone;
- Case 2: Load transfer representative of an average  $\beta = 1.0$  along casing interface; and,
- Case 3: Load transfer representative of an average  $\beta = 2.0$  along casing interface.

Note that the calculation of vertical effective stress includes a surcharge of 15 kPa for the concrete slab and a depth of water of 1.5 m. The results, shown in Table 2, indicate that the value of bond zone bond stress is not very sensitive to the assumption of resistance within the cased zone. The computed values of Beta range from 3.2 to 3.4 for the last load increment, which is consistent with values reported by Jeon and Kulhawy (2001). The value of Beta was not estimated based on the modified hyperbolic extrapolation, since the generation of end bearing resistance was suspected; the end bearing condition is discussed below. In light of the high axial stiffnesses inferred from Fig 4, the effects of the cased zone resistance do not appear to be adequately addressed by this method of analysis.

Another model used in analyzing micropile load test results is the elastic length concept described by Gomez, et al. (2003) and Cadden, et al. (2004), and illustrated in Fig 5(a). In this model, the elastic length,  $L_e$ , is equal to the product of the elastic micropile compression (deduced from elastic rebound) and the sum of the product of micropile Young's modulus and area for the micropile constituents ( $EA$ ), divided by the load decrement in an unload cycle. Bruce, et al. (1993), Gomez, et al. (2003), and Cadden, et al. (2004) suggest that the elastic length be used for estimating bond stress.

However, it is not apparent as to how to employ this model. It is not clear as to whether the cased zone should be ignored completely, or if not, how to incorporate the cased zone  $EA$  in light of the bond zone  $EA$ . The model shown in Fig 5(a) indicates partial load transfer through the cased zone, but no guidance is provided in selecting the amount of casing to include. Figure 6 shows the authors' estimate of the elastic length assuming load transfer through the full length of micropile and through the bond zone only. In both cases, this analysis technique would indicate no onset of end-bearing, which does not appear valid for the load test data presented herein. Gomez, et al. (2003) indicates that locked-in bond stresses may reduce the elastic recovery for tests conducted with load cycles, and therefore interpretation errors may occur.

Assuming Gomez, et al. (2003) and Cadden, et al. (2004) intended to ignore load transfer through the cased zone

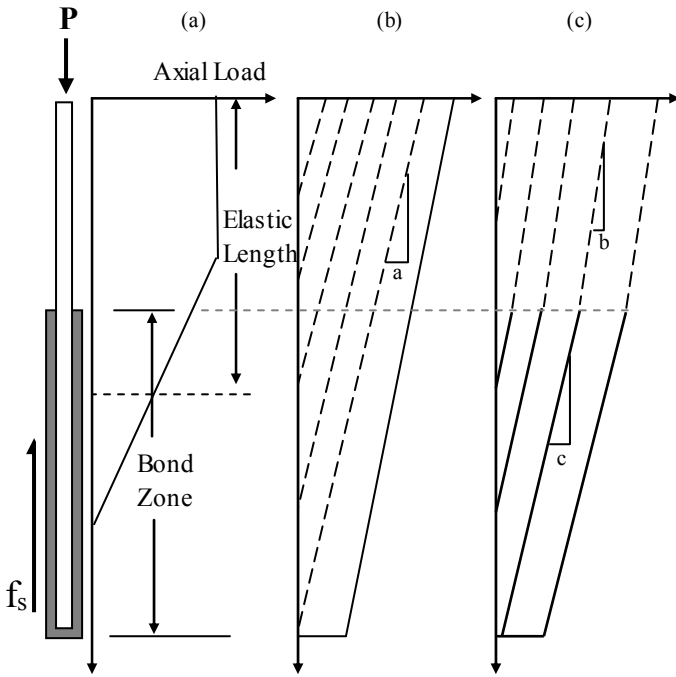


Fig. 5. Possible load transfer models: (a) elastic length concept (after Cadden, et al; 2004); (b) load transfer averaged across cased and uncased length; and (c) separate average load transfer for cased and uncased length.

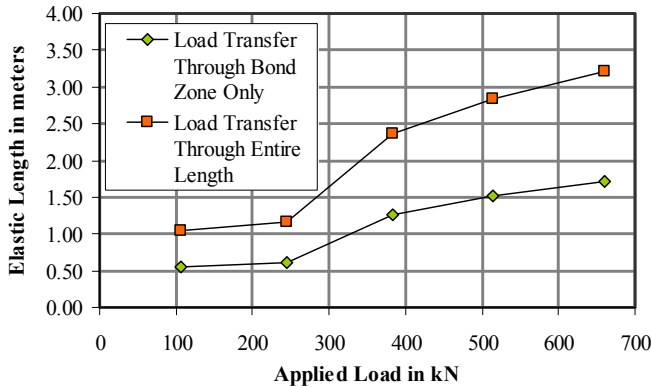


Fig. 6. Computed elastic length for compression load test.

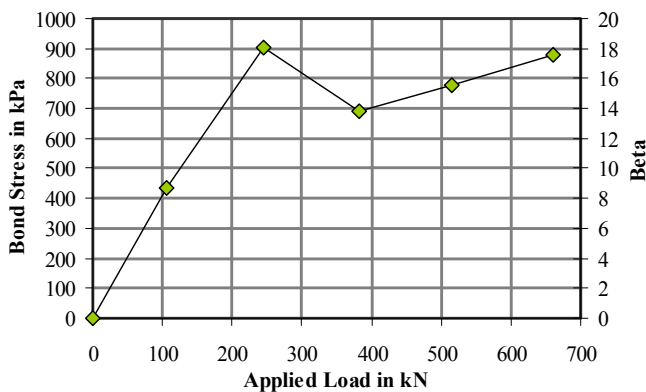


Fig. 7. Bond stresses estimated from elastic length method.

completely, one may estimate bond stresses. Fig 7 shows the computed bond stress and average Beta for the compression micropile. It is readily apparent that bond stresses estimated from the elastic length as determined within the bond zone only (ignoring load transfer through the cased length) produces bond stress estimates that are much greater than that reported within the literature for similar soil conditions.

#### Micropile Stiffness Degradation

The average bond stress may be calculated from the results of an uninstrumented micropile load test provided an estimate of the loaded length can be made reliably. Information regarding steel casing, steel reinforcement, bond zone diameter, and grout quality (i.e., Young's modulus of grout, or at a minimum compressive strength) are required to accurately estimate the loaded length of the micropile.

The global axial stiffness for any load increment,  $j$ , of the micropile may be assessed for each load cycle,  $i$ , by the following:

$$K_{i,j} = \frac{P_{i,j}}{\Delta_{i,j}} \quad (2)$$

where  $P$  and  $\Delta$  are the applied load and resulting displacement, respectively. Note that for each load cycle, any permanent set or residual movement observed from the load decrement for load cycle  $i - 1$  should be subtracted from the displacement from load cycle  $i$  in the stiffness calculation. For the purpose of comparison, the axial stiffness of the cased zone should be calculated from:

$$K_{cased} = \frac{(EA)_{casing} + (EA)_{reinforcement} + (EA)_{grout}}{L_{cased}} \quad (3)$$

and the axial stiffness of the bond zone should be estimated from:

$$K_{bond} = \frac{(EA)_{reinforcement} + (EA)_{grout}}{L_{bond}} \quad (4)$$

The weighted mean stiffness of the micropile may be estimated as:

$$K_{mean} = \frac{K_{bond}L_{bond} + K_{cased}L_{cased}}{L_{total}} \quad (5)$$

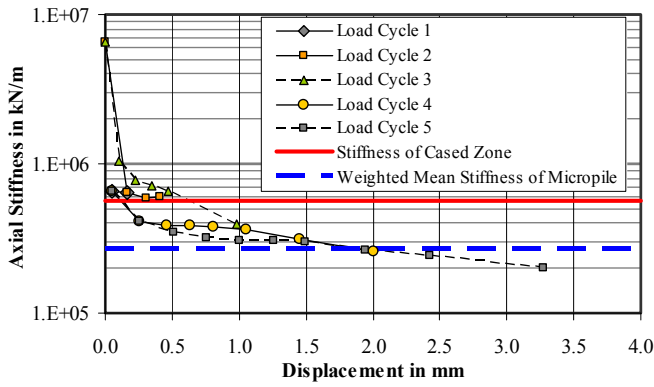


Fig. 8. Global stiffness degradation for compressive load test.

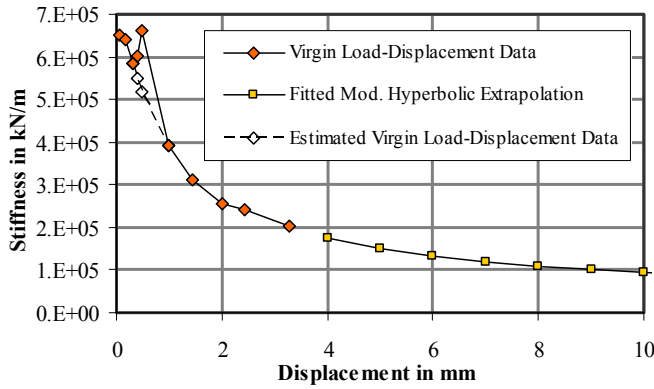


Fig. 9. Virgin global stiffness degradation curve for compressive load test.

The global axial stiffness calculated from the load displacement curve in Fig 3 and 4 is presented in Fig 8. Interestingly, load cycles 1 and 2 show global axial stiffnesses that are 50 percent greater than the elastic axial stiffness estimated for the cased length. This indicates that significant load transfer is occurring within the cased zone. Load cycles 2 and 3 indicate that the initial load cycling may even stiffen the surrounding soil, with initial global axial stiffnesses greater than that observed for load cycle 1 by an order of magnitude. Subsequent to load cycle 3, load appears to be shed within the bond zone as the global axial stiffness degrades to a value below the cased zone to some value greater than the weighted mean stiffness of the micropile, given by Eqn (5). Load cycles 3, 4, and 5 appear to collapse to a unique global stiffness degradation curve with increasing micropile head displacements, representative perhaps of global stiffness degradation during a hypothetical virgin load-displacement curve (estimated by the corrected load-displacement curve in Fig 4). Finally, the last axial stiffness value of load cycle 4 and last three values of axial stiffness for load cycle 5 appear to fall below that of the weighted mean axial stiffness of the micropile, indicating the development of end-bearing resistance.

The data from Fig 8 can be selectively plotted, as shown in Fig 9 to show only the values of global micropile stiffness

representative of an instance of virgin load, using the corrected load displacement curve in Fig 4. Fig 9 also provides the estimated global stiffness degradation curve from the fitted modified hyperbolic curve. Note that due to load cycling, some increase in soil stiffness occurred, likely along the cased zone, such that the global stiffness degradation curve may not truly represent the virgin load behavior. Therefore, two additional data points are estimated and plotted to show the expected stiffness degradation behavior for the virgin, monotonically loaded micropile.

### Global Stiffness Degradation Method

Given the global stiffness degradation data calculated from Eqn (2), one can then solve for an estimated loaded length with the following procedure:

1. Provide an initial guess for loaded length;
2. For the first value of global stiffness,
  - a. If the global stiffness calculated from Eqn (2) is less than the axial stiffness of the cased length, select the value of loaded length that minimizes the error between observed global stiffness and Eqn (3). Substitute the loaded length for  $L_{cased}$  in Eqn (3) for this step;
  - b. If the observed global stiffness is less than axial stiffness of the cased length, but more than the weighted mean axial stiffness, then estimate the observed global stiffness by:

$$K_{est} = \frac{K_{cased} L_{cased} + K_{mean} (L_{Loaded} - L_{cased})}{L_{Loaded}} \quad (6)$$

Select the value of loaded length that minimizes the error between the observed and estimated global stiffness;

- c. If the observed global stiffness is less the  $K_{mean}$ , then the micropile is loaded along the full length, and end bearing resistance has been engaged.
3. Repeat Step 2 for all values of observed global stiffness.

The global stiffness degradation method is very simple analytical tool for determining loaded length. Methods employing much greater sophistication exist to analyze micropile load-displacement behavior that includes the effects of soil-grout interface characteristics (e.g., Misra, et al, 2004). The assumptions required for the global stiffness degradation method for estimating loaded length include:

1. Young's modulus of the grout can be reliably estimated;
2. The diameter of the bond zone is known; and,
3. The micropile can be modeled with rigid-perfectly plastic interface behavior; this is similar to a free-

standing micropile resting on a rigid base with variable length during loading.

A strong limitation of this method is found in the estimation of the Young's modulus of the grout. The Young's modulus of the grout is dependent on the strain level within the grout (Fellenius, 1989); thus estimation of the micropile-specific variable secant Young's modulus requires the use of strain gages. Without this information, a tangent Young's modulus and/or secant Young's modulus or modulus degradation relationship must be estimated. Similarly, the diameter of the micropile bond zone is often difficult estimate reliably, providing additional error in the calculation of bond stress. Nonetheless, where an estimate of bond stress is required, a value of bond zone diameter must be estimated; the observed grout take volumes may provide assistance in the estimation of this parameter. Finally, the results of typical load transfer curves of instrumented piles and micropiles typically show that some amount of skin friction is mobilized along the entire length of a test pile with a very small amount of movement. The stiffness degradation method assumes a variable loaded length due to the rigid-perfectly plastic interface behavior.

Following the determination of the loaded length, an assumption regarding the load transfer function must be made. One may choose a simple load transfer function, where the decrease in load occurs at a constant rate across cased and uncased length, such as that shown in Fig 5(b). If there is evidence to justify a smaller rate of load decrease through the cased zone, one may elect the load transfer shown in Fig 5(c), where there is a separate average load transfer for the cased and uncased length. Additionally, assumptions regarding end-bearing resistance should be made. It is likely that micropiles develop a residual load due to the effects of steel elongation and subsequent constrained contraction during grout curing. However, the residual load is extremely difficult to estimate, even with strain gage instrumentation. However, the residual load that develops is likely to be smaller than that of augercast piles, which develop significantly less residual load than that of driven piles, due to interaction with the casing. Additional assumptions regarding end bearing resistance should be made, such as choosing at what percent of micropile head displacement to begin attributing load resistance to end bearing or to neglect end bearing until the observed stiffness falls below weighted mean stiffness. Following the selection of the start of the end bearing condition, one must decide what portion of additional load is resisted by skin friction, and what portion by end-bearing. This last point is fairly difficult to estimate, particularly in light of possible strain-softening interface behavior. The decision to neglect any end bearing resistance may result in the possible reversal of bond resistance degradation.

#### Calculated Loaded Length and Estimation of Bond Stress

The loaded length was calculated for all points of the observed and estimated load displacement data shown in Fig 9 in accordance with the global stiffness degradation method. The

last three observed data points produced a loaded length in excess of 8.23 m, the total length of the micropile. Therefore, the development of an end bearing condition is tacitly inferred (assuming accurate estimation of bond zone diameter and grout Young's modulus) for the last three load applications. The bond stress is estimated by dividing the applied load by the product of loaded length and micropile perimeter; this estimation assumes a load distribution as shown in Fig 5(b). Load transfer data presented by Holman and Barkauskas (2007) shows that the end-bearing percentage ranges from 20 to 33 percent of total applied load for granular material with similar relative density (as inferred from SPT testing). Based on this information, an end-bearing percentage of 25 percent is selected for bond stress estimation.

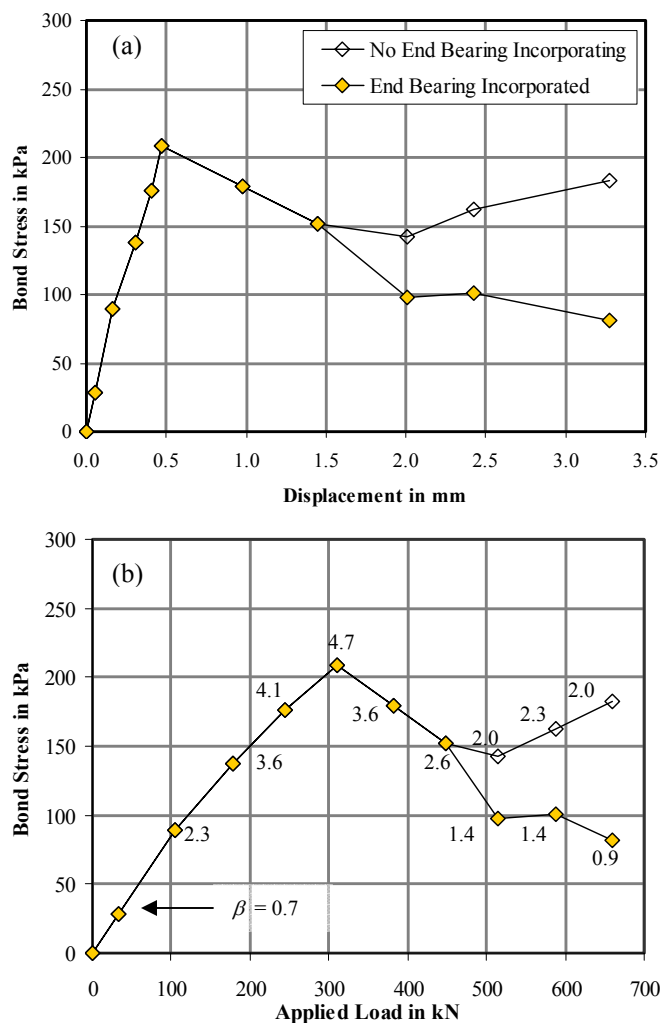


Fig. 10. Estimated bond stress for compression load test: (a) versus micropile head displacement, and (b) versus applied load.

Assuming a constant load transfer function, the bond stresses plotted in Fig 10 rapidly approaches a peak value with increasing micropile head displacement and applied load. Peak bond stresses occur at a head displacement of approximately 0.5 mm and 300 kN. The average Beta values are plotted for

each data point for reference and comparison to the previously presented analyses. For the case where the assumed end-bearing resistance of 25 percent of the total load is incorporated, the post-peak bond stress degrades at a decreasing rate with increasing micropile head displacement and applied load. It is likely that the granular soil adjacent to the grout-to-ground interface initially experiences dilation, followed by a reduction in bond resistance as the adjacent material approaches a constant-volume state of frictional resistance with continued deviatoric interface strain. For the case where no end bearing resistance is incorporated, a case in disagreement with the evidence presented in Fig 3, the additional loading causes a reversal in the degradation of bond stress. Neglecting end-bearing in medium dense to dense sands and gravels, therefore, may cause overestimation of bond stress resistance.

The global stiffness degradation method, while making many simplifying assumptions, appears to reveal fairly complicated load transfer behavior. The evidence for post-peak bond strength reduction for micropiles is not new. Gomez, et al (2003) and Cadden, et al. (2004) discuss post-peak reductions in grout-to-ground bond strength, where evidence was provided for several segments along a micropile length. The global stiffness degradation method, while crude, appears to provide additional argument for the potential for strain-softening bond resistance.

## ANALYSIS OF THE TENSION LOAD TEST

### Uplift Micropile Behavior

The load displacement curve for the micropile load test performed in tension is shown in Fig 3, where significant deviation in behavior from the micropile loaded in compression is apparent. The initial portion of the load displacement curve appears to be concurrent with that of the compression test up to a load of approximately 179 kN (40 kips), whereupon a relatively constant, but significantly less stiff, load displacement behavior occurs. The last load increment just prior to unloading indicates that an ultimate uplift resistance may have been imminent.

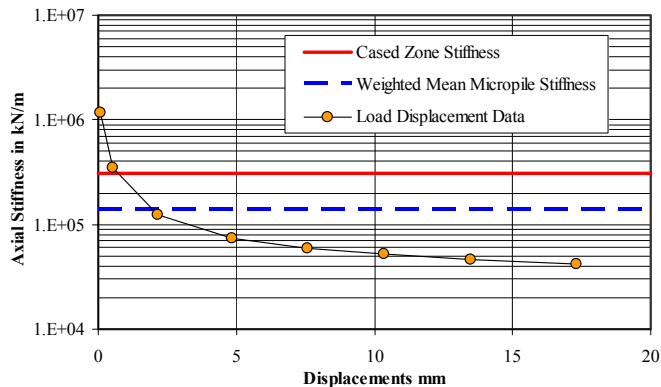


Fig. 11. Global stiffness degradation curve for tension load test.

Figure 11 shows the global stiffness degradation curve for the tension test; note, the cased zone and weighted mean micropile stiffness shown for comparison reflects the stiffness of the steel portions of the cross section only, per the FHWA guidelines (FHWA, 2005). From Fig 11, it is apparent that: (1) the bond zone becomes fully loaded fairly quickly, within the third load increment, and (2) the first two load increments are resisted largely by the cased zone, indicating again that load transfer within the cased zone likely occurs.

The bond stress development for the tension load test is expected to occur somewhat differently than that for the compression load test, not only due to the lack of an end-bearing development, but also due to the Poisson effect within the casing. The loaded length was determined using the global stiffness degradation method, which was then used to determine the bond stresses. Figure 12 shows four potential scenarios of bond stress development for the tension load test.

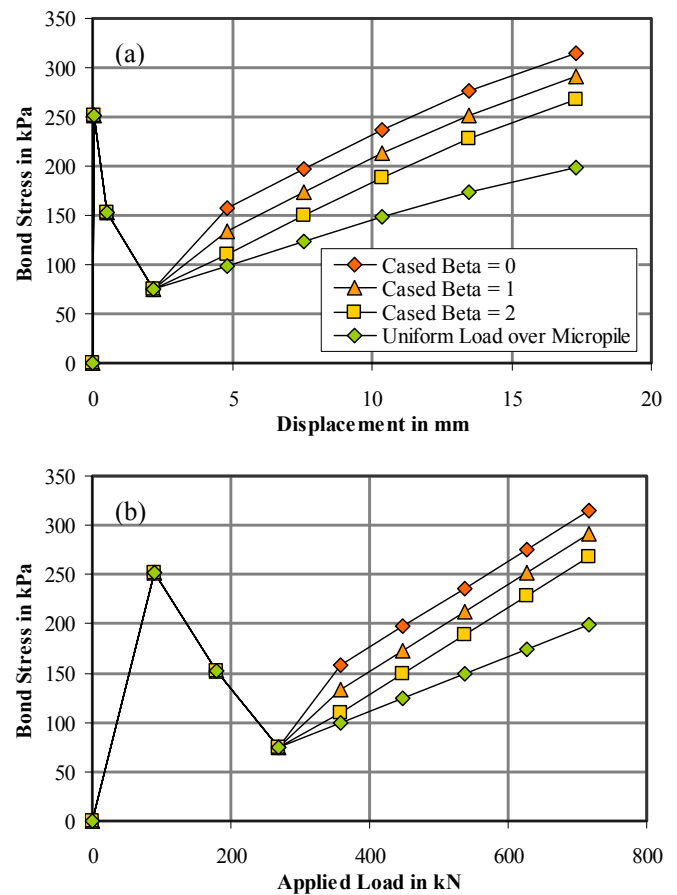


Fig. 12. Estimated bond stresses for tension load test: (a) versus micropile head displacement, and (b) versus applied load.

The four scenarios are similar up to the third load increment since the full loaded length is used to calculate the bond stress (including load transfer within the cased zone). Subsequent to the third load increment, one may assume that either no load

transfer occurs within the cased length ( $\beta = 0$ ), that load transfer occurs at some ratio of vertical effective stress ( $\beta = 1$  or  $2$ ) per Fig 5(c), or a uniform load transfer function over the full length of the micropile, per Fig 5(b). The assumption of neglecting all initial load transfer within the cased zone does not appear to be valid given the very high value of initial global stiffness; this scenario was therefore not considered.

For the four load transfer scenarios considered, Figure 12 shows that there is an initial value of bond resistance, within the cased length, of 250 kPa. This bond resistance is followed by a reduction of 70 percent to approximately 75 kPa, representative of a  $\beta$  equal to 2. The initial decrease reflects a rapid loss of resistance along the cased length of the micropile, perhaps exacerbated by the radial contraction of casing under tension. This Poisson effect may reduce radial earth pressures around the cased zone, although the grout within the casing likely prevents most, if any, contraction. Subsequently, the bond zone becomes loaded along its full length, with an increase in bond stress with increasing micropile head displacement.

Of the four load transfer scenarios considered, it appears that the scenarios considering a high rate of load transfer within cased zone brackets the peak bond stress observed in the compressive load test at the last observed load increment in the tension test. This indicates, in light of potential imminent ultimate pullout resistance, that an ultimate  $\beta$  equal to two or more may provide a good estimate of load transfer within the cased zone in a tension test, for medium dense to dense sands and gravels, following the post-peak strength reduction along the cased length under uplift loading.

## DISCUSSION

The two load tests presented and analyzed above are useful for comparison, in that they are installed within the same subsurface, are constructed to the same specifications (i.e., diameter, cased length, bond length, elevations, etc.), and show different behavior for compression and tension. For example, at the design load of 360 kN (80 kips), the tension test produced 5 times the head displacement of the compression test. This ratio of displacements holds approximately constant throughout the range of applied loads.

Both the compression and the tension load tests indicate that some amount of load transfer occurs within the cased length when analyzed with the stiffness degradation method. Comparison of these two load tests and analysis by the stiffness degradation method indicate that end bearing resistance has been developed at the toe of the micropile loaded in compression. Methods ignoring load transfer within the cased zone and end bearing resistance may not allow adequate estimation of bond stresses.

The practicing consultant should employ instrumentation to observe the actual load transfer rates, particularly where significant economic benefit may result. Unfortunately,

opportunities for the installation and use of instrumentation are not as frequent as desired. Within the stated limitations, which are not unsubstantial, the stiffness degradation method may provide an alternative estimate of bond stresses, and information regarding the transfer of load through the casing and the development of an end bearing condition.

## CONCLUSIONS

Micropile foundations provided an alternative to augercast piling at the paper plant of Nippon Paper Industries USA Company. The micropiles were installed in two separate upgrades within medium dense to dense, gravelly sand beach and advance outwash deposits. Comparison of two tested micropiles, one in compression and one in tension, indicated the development of end bearing within the micropile loaded in compression. Analysis of both the compression and the tension load test with the stiffness degradation technique indicate that load is transferred within the cased zone. Several methods were used to estimate bond stresses for the compression load test. Methods ignoring load transfer through the cased zone and the development of end bearing resistance may not have provided the most reliable estimate of bond stress.

## ACKNOWLEDGEMENTS

The author's would like to thank Nippon Paper Industries USA Co., and particularly Ralph Renes and Dean Reed, for sharing plant information and allowing the dissemination of the presented data. Alan Jones, formerly of Hart Crowser, Inc., assisted in managing Upgrade 1.

## REFERENCES

- Armstrong, J.E., Crandell, D.R., Easterbrook, D.J., and Noble, J.B. [1965] "Late Pleistocene Stratigraphy and Chronology in Southwestern British Columbia and Northwestern Washington," *Geologic Society of America Bulletin*, Vol. 76. pp 321-330.
- Booth, D.B. [1987] "Timing and Processes of Deglaciation Along the Southern Margin of the Cordilleran Ice Sheet," *North America and Adjacent Oceans During the Last Glaciation*, Ruddiman, W.F., and Wright, H.E., Eds, Geology of North America, Vol. K-3, Geologic Society of America, Boulder, Colorado. pp. 71-90
- Cadden, A., Gómez, J., Bruce, D., and Armour, T. [2004] "Micropiles: Recent Advances and Future Trends," *Current Practices and Future Trends*, GSP No. 125, ASCE, Reston, Virginia. 27 pp.
- Downing, J. [1983] "The Coast of Puget Sound—Its Processes and Development," *Puget Sound Books*, Washington Sea Grant/Univ. of Washington Press, Seattle, WA.

Fellenius, B. H. [1989] "Tangent Modulus of Pile Determined From Strain Data," *Foundation Engineering Congress, Symposium on Predicted and Observed Behavior of Piles*, GSP No. 23, ASCE, R.J. Finno, Ed., Reston, Virginia. pp. 293-302.

Galster, R.W. [1989] "Ediz Hook—A Case History of Coastal Erosion and Mitigation," *Engineering Geology in Washington*, Vol. II., R.W. Galster, Ed., Washington Division of Geology and Earth Resources, Bulletin 78. p.1177-1186

Gómez, J.E., Cadden, A.W., and Bruce, D.A. [2003] "Micropiles in Rock: Development and Evolution of Bond Stresses under Repeated Loading," 12<sup>th</sup> Pan-American Conference on Soil Mechanics and Geotechnical Engineering, Cambridge, MA.

Han, J., and Ye, S.-L. [2006] "A Field Study on the Behavior of Micropiles in Clay under Compression or Tension," *Canadian Geotechnical Journal*, Vol. 43, No. 1, NRC Research Press, Canada. pp. 19-29

Holman, T.P., and Barkauskas, B.D. [2007] "Mechanics of Micropile Performance from Instrumented Load Tests," *Field Measurements in Geomechanics 2007*, GSP No. 176, ASCE, J. DiMaggio and P. Osborn, Eds., Reston, Virginia. 14 pp.

Jeon, S.S., and Kulhawy, F. H. [2001] "Evaluation of Axial Compression Behavior of Micropiles," *Foundations and Ground Improvement*, GSP No. 113, T.L. Brandon, Ed., ASCE, Reston, Virginia. pp. 460-471.

Misra, A., Chen, C.-H., Oberoi, R., and Kleiber, A. [2004] "Simplified Analysis Method for Micropile Pullout Behavior," *Journal of Geotechnical and Geoenvironmental Engineering*, Vol. 130, No. 10, ASCE, Reston, Virginia. 1024- 1033.

Porter, S.C., and Swanson, T.W. [1998] "Radiocarbon Age Constraints on Rates of Advance and Retreat of the Puget Lobe of the Cordilleran Ice Sheet During the Last Glaciation," *Quaternary Research*, Vol. 50. p 205-213

Zhu, H., and Chang, M.-F. [2002] "Load Transfer Curves along Bored Piles Considering Modulus Degradation," *Journal of Geotechnical and Geoenvironmental Engineering*, Vol. 128, No. 9, ASCE, Reston, Virginia. pp 764-774.